Inorganic Chemistry

ARTICLE

pubs.acs.org/IC

First-Row Transition-Metal Chloride Complexes of the Wide Bite-Angle Diphosphine ^{iPr}DPDBFphos and Reactivity Studies of Monovalent Nickel

Elodie E. Marlier, Stephen J. Tereniak, Keying Ding, Jenna E. Mulliken, and Connie C. Lu*

Department of Chemistry, University of Minnesota, 207 Pleasant Street SE, Minneapolis, Minnesota 55455-0431, United States

Supporting Information

ABSTRACT: The diphosphine 4,6-bis(3-diisopropylphosphinophenyl)dibenzofuran (abbreviated as ^{iPr}DPDBFphos) has been metalated with transition metal dichlorides of zinc, cobalt, and nickel to yield (^{iPr}DPDBFphos)MCl_2 complexes. Within these compounds, the diphosphine ^{iPr}DPDBFphos adapts a wide range of bite angles (115 to 180°) as determined by X-ray crystallography. A three-coordinate planar Ni(I) species was isolated from the reduction of (^{iPr}DPDBFphos)$NiCl_2$ with KC_8. Low-temperature electron paramagnetic resonance (EPR) measurements of (^{iPr}DPDBFphos)NiCl allow the determination of g values (2.09, 2.14, 2.37) and hyperfine coupling constants to two ^{31}P nuclei, $A_{iso} = 46 \times 10^{-4}$ cm^{-1}, and one ^{37}Cl/^{35}Cl nucleus, $A = (12, 0.7, 35) \times 10^{-4}$ cm^{-1}. Density functional theory (DFT) studies reveal the nature of the magnetic orbital to be d_{xy}, which has σ-antibonding and $\pi_{\|}$-antibonding interactions with the phosphorus and chloride atoms, respectively. The monovalent nickel complex reacts with substrates containing C−X bonds; and in the case of vinyl chloride, a Ni(II) vinyl species (^{iPr}DPDBFphos)Ni(CH=CH$_2$)Cl is generated along with the Ni(II) dichloride complex. The monovalent Ni(I) chloride is an active catalyst in the Kumada cross-coupling reaction of vinyl chloride and phenyl Grignard reagent.

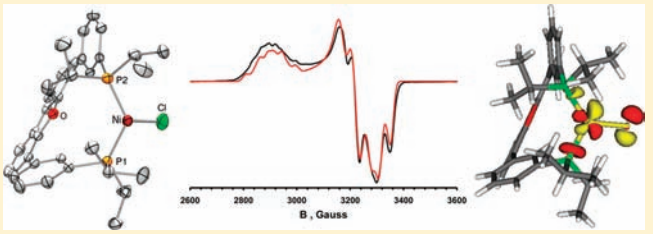

I. INTRODUCTION

In homogeneous transition-metal catalysis, the reactivity of the metal center is often fine-tuned by modifications to the supporting ligand(s). The development of ligand scaffolds becomes invaluable when these scaffolds confer new reactivities at the metal center that result in advances in catalysis. We have reported a conformationally flexible diphosphine, ^{iPr}DPDBFphos, shown in Chart 1 and its *cis*- and *trans*-coordination complexes of Rh(I) and Pd(II).[1] The ligand ^{iPr}DPDBFphos is analogous to 4,6-bis(diphenylphosphino)dibenzofuran (DBFphos)[2,3] but has an aryl linker between the dibenzofuran backbone and the phosphine donors. One effect is to distance the backbone from the transition metal center, and hence, to prevent binding of the O-atom to the metal. Another effect is to confer flexibility to the ligand's chelate properties.[4,5] Specifically, ^{iPr}DPDBFphos supports a wider range of bite angles within coordination complexes (compared to DBFphos, whose bite angle is limited to 150−157°)[6,7] and can switch from the *cis* to *trans* coordination mode with a calculated 3.5 kcal/mol driving force.[1]

Herein, we extend the coordination chemistry of ^{iPr}DPDBFphos to the first-row transition metals zinc, cobalt, and nickel. A long-standing goal in homogeneous catalysis is to replace precious transition-metal catalysts with their earth-abundant counterparts.[8,9] Notable organometallic examples include iron-mediated cross-coupling reactions,[10] hydroxylation of aliphatic C−H bonds,[11−14] and hydrogenation of alkenes[15−17] and ketones;[18,19] cobalt-mediated hydroformylation[20] and cross-coupling;[21] and nickel-mediated polymerization and oligomerization of olefins,[22−24] cross-coupling,[25,26] and cyclization reactions.[27] More relevant to the complexes reported here, P_2MX_2-type complexes of cobalt and zinc have been shown to be effective catalysts for the polymerization of methyl acrylate and CO_2/ethylene oxide, respectively.[28,29]

The (^{iPr}DPDBFphos)MCl_2 complexes are characterized by UV−visible (UV−vis) spectroscopy, heteronuclear NMR spectroscopies, and single-crystal X-ray diffraction studies. A three-coordinate nickel(I) chloride complex is presented with additional

Chart 1. Ligands DBFphos and ^{iPr}DPDBFphos

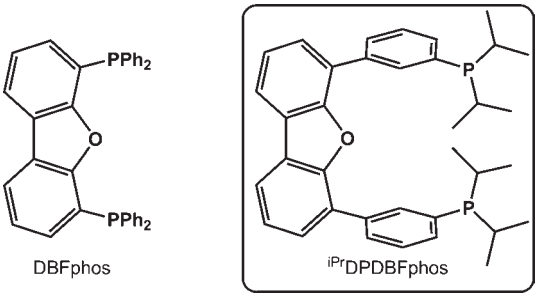

Received: March 23, 2011
Published: August 31, 2011

Scheme 1. Synthetic Routes to Coordination Complexes 1 to 4

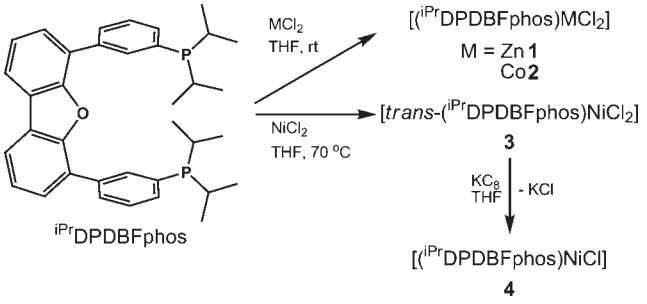

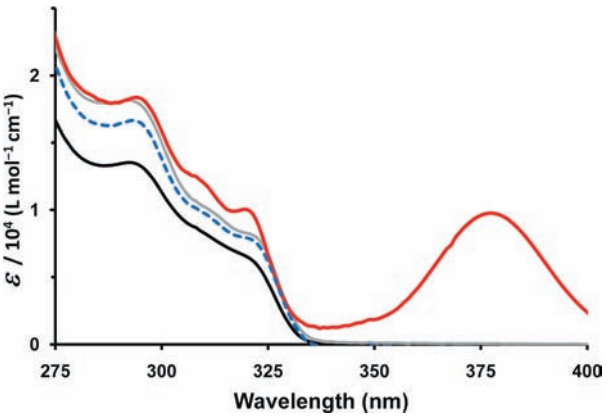

Figure 1. Electronic absorption spectra of Zn **1** (black solid line), Co **2** (blue dashed line), Ni **3** (red solid line), and ^{iPr}DPDBFphos (gray solid line) in THF at ambient temperature.

characterization from electron paramagnetic resonance (EPR) spectroscopy and density functional theory (DFT) calculations. Preliminary reactivity studies of the nickel(I) chloride have been conducted, and our results join recent studies in demonstrating the relevance of isolated monovalent nickel species in cross-coupling catalysis.[30,31]

II. RESULTS AND DISCUSSION

Syntheses of (^{iPr}DPDBFphos)MCl$_2$, where M = Zn, Co, Ni. The diphosphine ligand ^{iPr}DPDBFphos is cleanly metalated with the anhydrous transition metal dichlorides as shown in Scheme 1 to provide the zinc, cobalt, and nickel dichloride complexes, [(^{iPr}DPDBFphos)ZnCl$_2$] **1**, [(^{iPr}DPDBFphos)CoCl$_2$] **2**, and [*trans*-(^{iPr}DPDBFphos)NiCl$_2$] **3**, respectively.

UV−vis and NMR Spectroscopic Characterization of (^{iPr}DPDBFphos)MCl$_2$, where M = Zn, Co, Ni. The UV−vis spectra of compounds **1**−**3** were collected at room temperature in tetrahydrofuran (THF). All complexes have characteristic bands in the UV region from 275 to 330 nm (Figure 1, Supporting Information, Table 1S). These bands are intense ($\varepsilon \sim 10^4$ L mol^{-1} cm^{-1}) and do not shift significantly for the different transition metal ions. These excitations primarily originate from the dibenzofuran group since the ligand ^{iPr}DPDBFphos has analogous absorbances in this range. Between 330 and 800 nm, the colorless zinc complex **1** has no absorbances, which is consistent with its d^{10} electron count (Figure 2). The brilliant blue cobalt complex **2** has several bands between 550 and 800 nm with molar absorptivity values between 320 and 530 L mol^{-1} cm^{-1} (Supporting

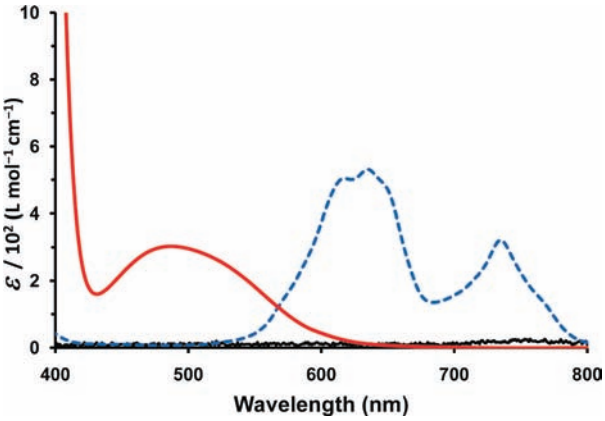

Figure 2. Electronic absorption spectra of Zn **1** (black solid line), Co **2** (blue dashed line), and Ni **3** (red solid line) in THF at ambient temperature.

Information, Figure 1S), which are typical of d-d transitions of a high-spin Co(II) center. The bright red nickel complex **3** has a prominent, intense transition with a maximum at 377 nm (ε = 9,500 L mol^{-1} cm^{-1}, Supporting Information, Figure 2S) and overlapping broad features from 420 to 600 nm ($\varepsilon \sim$ 300 L mol^{-1} cm^{-1}).[32] The broad features are likely d-d transitions, while the intense peak is tentatively assigned as a ligand-to-metal charge transfer band.

Compounds **1**−**3** have been characterized by NMR spectroscopy. For the two diamagnetic complexes, Zn **1** and Ni **3**, one type of phosphorus nucleus is observed at 2.7 and 26.5 ppm, respectively. In the corresponding ^{1}H NMR spectrum of **1** (Supporting Information, Figure 3S), half of the aryl protons of the ligand are unique, consistent with the approximate 2-fold symmetry observed in its solid-state structure (vide infra). For the four isopropyl groups of the ligand, only one methine proton and two methyl resonances are seen. This is an unexpected observation since a 2-fold axis should result in two chemically distinct methine types. Hence, their full equivalency must be rationalized by another mechanism (vide infra).

At room temperature, the ^{1}H NMR spectrum of the nickel compound **3** contains both sharp and broad resonances (Figure 3). The sharp signals correspond to the dibenzofuran group, while those belonging to the isopropyl groups and the aryl linkers are significantly broadened. Upon cooling to −45 °C, the ^{1}H NMR spectrum of **3** sharpens completely, and exactly half of the protons of the ligand are uniquely observed, consistent with the approximate mirror-plane symmetry of its molecular structure. At low temperature, the isopropyl groups resolve into two distinct methine and three methyl resonances. The presence of the mirror plane means that the two chemically different methine protons occur within the same phosphine group, that is, P(CHMe$_2$)(C′HMe$_2$). If P−C$_{methine}$ bond rotation is fast, then two methyl peaks would be expected; if slow, four. At −45 °C, only three methyl signals are apparent because of a coincidental overlap of two of the four possible methyl peaks.[33] At room temperature, the ^{1}H NMR spectrum of **3** shows one methine and two methyl signals, akin to that of **1**. Again, the higher symmetry solution structure cannot be explained by a mirror plane alone. Additional fluxional processes will be described in the next section.

The cobalt dichloride compound **2** is characterized by a paramagnetic ^{1}H NMR spectrum, which is consistent with a

dx.doi.org/10.1021/ic200589e |*Inorg. Chem.* 2011, 50, 9290–9299

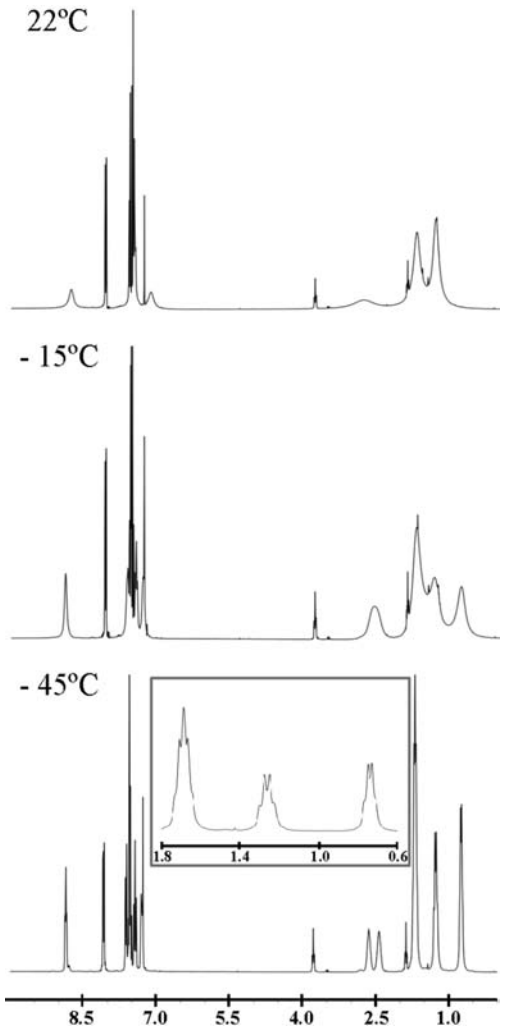

Figure 3. Variable-temperature ^{1}H NMR spectra (300 MHz, $CDCl_3$) of [*trans*-(^{iPr}DPDBFphos)$NiCl_2$] **3**. Inset is an expansion of the methyl region at −45 °C.

Co(II) oxidation state. Its solution magnetic moment of μ_{eff} = 4.01 μ_B is slightly greater than the spin-only magnetic moment for an $S = 3/2$ state ($\mu_{S.O.} = 3.88\,\mu_B$), which leads to the expected assignment of a high-spin Co(II) center.

Solid-State Structures of (^{iPr}DPDBFphos)MCl_2, Where M = Zn, Co, Ni. Crystallographic data are provided in Table 1, and selected bond lengths and angles are collected in Table 2. The geometry of the zinc and cobalt centers in **1** and **2**, respectively, are tetrahedral. The structures of **1** and **2** are highly homologous as shown in Figures 4 and 5, and their unit cell dimensions are nearly identical. Both structures contain an approximate 2-fold rotation axis. The P-M-P bond angles are 115.27(3)° and 114.62(2)° in the zinc and cobalt complexes, respectively. Previously, we observed a more acute bite angle of 104.5° for ^{iPr}DPDBFphos in the distorted square planar complex [*cis*-(^{iPr}DPDBFphos)Rh(nbd)]BF_4.[1] The Co−P and Zn−P bond distances in **1** and **2**, respectively, are comparable to other diphosphine dichloride coordination complexes with the corresponding transition metal centers.

The geometry of the nickel center in **3** is square planar with a *trans*-spanning ^{iPr}DPDBFphos ligand (P−Ni−P = 176.55(2)°) as shown in Figure 6. The Ni−P bond distances in **3** (2.2410(5), 2.2413(5) Å) are unremarkable compared to other *trans*-diphosphine nickel dichloride complexes (average P−Ni = 2.24 Å, Cambridge Structural Database).[6,7] An approximate mirror plane bisects the solid-state structure of **3**. The two chloride atoms in **3** reside in the mirror plane and are nonequivalent. One chloride is near the dibenzofuran backbone while the other chloride is sandwiched between the isopropyl substituents. At room temperature, the ^{1}H NMR peaks representing the isopropyl groups coalesce into one methine and two methyl resonances. The coalescence requires a combination of two dynamic motions illustrated in Scheme 2: (1) canting of the aryl linkers, which flips the relative bent orientation of the dibenzofuran group, and (2) rotation of the P−Ni−P vector, equalizing the two chlorides. Similar fluxional behavior has been previously described for the analogous square-planar complexes, [*trans*-(^{iPr}DPDBFphos)Rh(NCMe)$_2$]BF_4 and [*trans*-(^{iPr}DPDBFphos)Pd(NCMe)$_2$]$(BF_4)_2$.[1] We propose that canting of the aryl linkers would also occur in tetrahedral **1** to rationalize the solution-structure equivalency of all the methine protons of the ligand.

Synthesis and Characterization of (^{iPr}DPDBFphos)Ni^{I}Cl. The redox properties of compounds **1**−**3** were investigated by cyclic voltammetry (0.1 M [^{n}Bu$_4$N]PF_6 in THF), but no reversible redox events were found (Supporting Information, Figure 4S). Interestingly, the nickel dichloride complex **3** exhibited two irreversible events when scanning cathodically, whereas only one reductive signal was seen for the zinc and cobalt dichloride complexes, presumably a ligand-based reduction. Therefore, the chemical reduction of compound **3** was investigated. Sodium-based reducing agents such as sodium metal, sodium amalgam, and sodium naphthalide resulted in decomposition of **3** and formation of the free ligand by ^{31}P NMR spectroscopy. Mixing potassium graphite with **3** in THF resulted in an immediate color change from red to yellow (Figure 7). The resulting product is paramagnetic, and a single-crystal X-ray diffraction study reveals a three-coordinate, formally 15-electron Ni(I) complex, [(^{iPr}DPDBFphos)]NiCl **4** as shown in Figure 8.

Three-coordinate nickel complexes constitute a rich area in coordination chemistry. Supported by the bulky monophosphine PCy_3, zerovalent nickel forms adducts with small-molecules, as observed in the end-on dinitrogen dinickel compound {$(PCy_3)_2$Ni}$_2(\mu$-$N_2)$[34] and the first structurally characterized carbon-dioxide complex, $(PCy_3)_2Ni(\eta^2$-$CO_2)$.[35] Hillhouse has pioneered the area of divalent Ni=E complexes featuring multiply bonded ligands (E = NR, PR, CR_2) using the bulky diphosphine, 1,2-bis(di-*tert*-butylphosphino)ethane.[36−38] Other notable three-coordinate nickel complexes have been supported by nontraditional phosphine ligands, including the Fryzuk-type tridentate bis(phosphine)amides,[39] diketiminates,[40−42] *N*-heterocyclic carbenes,[43,44] and the unusual *N*-heterocyclic silenes.[45] Typically, the oxidation state of the nickel center is monovalent for the anionic ligands, and zerovalent for the neutral carbenes/silenes. The rare Ni(III) oxidation state has also been proposed in three-coordinate Ni(III) imides, which can be remarkably reactive and decompose via radical pathways.[46,47]

Yellow crystals of [(^{iPr}DPDBFphos)]NiCl **4** were grown from a concentrated CD_3CN solution at room temperature. Two independent molecules of **4** are found in the unit cell. Both nickel centers are three-coordinate and planar. The L−Ni−L angles sum to 359 and 360°. There are, however, significant variations in the bond and angle metrics between these two molecules (Table 2, A and B). For instance, the Ni−L bond distances within the two molecules differ from each other by 0.02 to 0.03 Å.

dx.doi.org/10.1021/ic200589e |*Inorg. Chem.* 2011, 50, 9290–9299

Table 1. Crystallographic Data for 1−4 and 6

	1	2	3	4	6
chemical formula	$C_{36}H_{42}Cl_2ZnOP_2$	$C_{36}H_{42}Cl_2CoOP_2$	$C_{36}H_{42}Cl_2NiOP_2$	$C_{36}H_{42}ClNiOP_2$	$C_{38}H_{45}ClNiOP_2$
formula weight	688.98	682.50	682.27	646.81	673.84
crystal system	triclinic	triclinic	monoclinic	monoclinic	triclinic
space group	$P\bar{1}$	$P\bar{1}$	$P2_1/c$	$P2_1/c$	$P\bar{1}$
a (Å)	9.772(3)	9.772(1)	19.181(3)	24.277(4)	11.952(3)
b (Å)	10.024(3)	10.020(1)	9.059(1)	17.431(3)	15.245(3)
c (Å)	17.882(6)	17.939(2)	21.040(3)	16.052(3)	20.695(5)
α (deg)	80.286(5)	80.377(2)	90	90	88.084(3)
β (deg)	75.748(5)	76.006(1)	115.196(2)	105.405(2)	73.958(2)
γ (deg)	85.834(5)	85.940(2)	90	90	89.567(3)
V (Å^3)	1672.6(9)	1679.5(3)	3308.0(8)	6549(2)	3622(1)
Z	2	2	4	8	4
D_{calcd} (g cm^{-3})	1.368	1.350	1.370	1.312	1.236
λ (Å), μ (mm^{-1})	0.71073, 1.017	0.71073, 0.793	0.71073, 0.873	0.71073, 0.799	0.71073, 0.725
T (K)	173(2)	173(2)	123(2)	173(2)	123(2)
θ range (deg)	1.19 to 26.37	1.18 to 27.52	1.17 to 27.49	1.46 to 26.37	1.71 to 26.51
reflns collected	16699	20155	31527	56856	26923
unique reflns	6815	7590	7531	13372	14614
data/restraint/parameters	6815/0/387	7590/0/387	7531/0/387	13372/0/755	14614/0/775
R_1, wR_2 ($I > 2\sigma(I)$)	0.0428, 0.0959	0.0372, 0.0830	0.0295, 0.0669	0.0540, 0.0904	0.0563, 0.1406

Table 2. Experimental Bond Distances (Å) and Angles (deg) for 1−4

				4, Ni(I)[a]	
	1, Zn(II)	2, Co(II)	3, Ni(II)	*A*	*B*
Bond Distances					
M−P(1)	2.420(1)	2.3920(7)	2.2410(5)	2.209(1)	2.233(1)
M−P(2)	2.416(1)	2.3844(7)	2.2413(5)	2.217(1)	2.243(1)
M−Cl(1)	2.255(1)	2.2331(7)	2.1748(5)	2.163(1)	2.180(1)
M−Cl(2)	2.2641(9)	2.2435(7)	2.1609(5)		
Bond Angles					
P(1)−M−P(2)	115.27(3)	114.62(2)	176.55(2)	115.53(4)	119.49(4)
Cl(1)−M−Cl(2)	117.38(3)	118.55(3)	175.10(2)		

[a] Two values are reported because two independent molecules (*A*, *B*) are present in the unit cell.

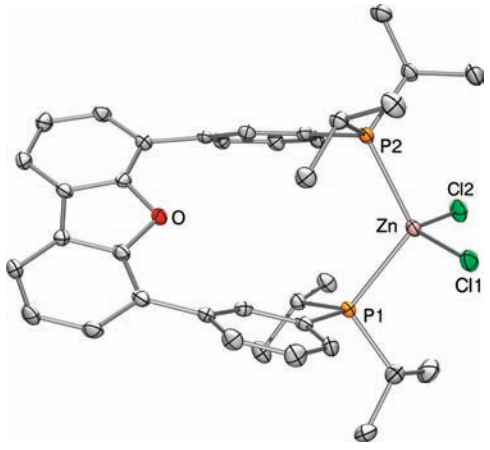

Figure 4. Solid-state structure of the [(^{iPr}DPDBFphos)$ZnCl_2$] **1** at 50% probability level. Hydrogen atoms were omitted for clarity.

One may normally expect to see a shortening of Ni−P bonds upon reduction of the Ni center (from **3** to **4**) because of increased π-back bonding into the phosphine ligands. However, this is not necessarily the case here. While molecule *A* does have significantly shorter Ni−P bond lengths relative to [*trans*-(^{iPr}DPDBFphos)$NiCl_2$] **3**, molecule *B* has essentially identical Ni−P bond lengths to those in **3**. The diphosphine bite angle in molecule *A*, 115.53(4)°, is nearly identical to that in the tetrahedral [(^{iPr}DPDBFphos)MCl_2] compounds reported here, but molecule *B* has a wider bite angle of 119.49(4)°. Moreover, the Ni*A* center is nearly trigonal planar with similar P(1)−Ni*A*−Cl and P(2)−Ni*A*−Cl bond angles of 122.94(4) and 121.53(4)°, respectively. The Ni*B* center has a more distorted trigonal geometry with the chloride ligand positioned asymmetrically between the two phosphorus atoms. The P(1)−Ni*B*−Cl and P(2)−Ni*B*−Cl bond angles are quite different at 104.61(4) and 135.00(4)°, respectively. The origin of the distortion is unclear. We looked for indications of crystal packing forces, but the shortest nonbonded contact distances to the chloride atom in the more distorted molecule (*B*) are too long (>2.88 Å for Cl----H)[48] to have much impact (Supporting Information, Table 2S).[49] Of relevance, the molecular structure of Ni(PPh_3)$_2$Cl is slightly distorted trigonal planar, and the observed asymmetry was attributed to a first-order Jahn−Teller effect.[50] This rationale, however, is inherently flawed because no degenerate d-orbitals can exist for NiP_2X species, even with idealized D_{2h} symmetry. Instead, we propose that the chloride atom wiggles within the NiP_2-plane, and that these structural perturbations cost little energy.

The X-band EPR spectrum of **4** in frozen toluene at 20 K is shown in Figure 9. A slightly rhombic signal is observed with *g*-values of 2.09, 2.14, and 2.37 (g_{iso} = 2.20), which are consistent with the assignment of a $S = 1/2$ Ni(I) center.[40,51,52] EPR spectra

dx.doi.org/10.1021/ic200589e |*Inorg. Chem.* 2011, 50, 9290–9299

of three-coordinate Ni(I) complexes typically have rhombic anisotropy with $g_3 - g_2 > g_2 - g_1$.[46,53] The spectrum was fitted using hyperfine coupling constants to two ^{31}P ($I = 1/2$) nuclei of $(43, 40, 55) \times 10^{-4}$ cm^{-1} ($A_{iso} = 46 \times 10^{-4}$ cm^{-1}) and to one $^{37}Cl/^{35}Cl$ nucleus ($I = 3/2$, abundance ratio = 0.3196) of $(12, 0.7, 35) \times 10^{-4}$ cm^{-1}. Large hyperfine coupling constants to the two ^{31}P nuclei are observed for all three g-values, while the hyperfine splitting caused by $^{37}Cl/^{35}Cl$ coupling is significant only for g_3. The equivalence of the two phosphorus nuclei in the frozen solution EPR of **4** stands in contrast to the classical work of Nilges et al. on the single-crystal EPR study of Ni(I)-doped Cu$(PPh_3)_2Cl$, in which the hyperfine coupling constants of the two phosphorus nuclei are remarkably inequivalent, $A_{iso}(^{31}P) = 38$ and 59×10^{-4} cm^{-1}.[54] Of note, our ^{31}P hyperfine coupling constant is midway between these two values determined for Ni$(PPh_3)_2Cl$.

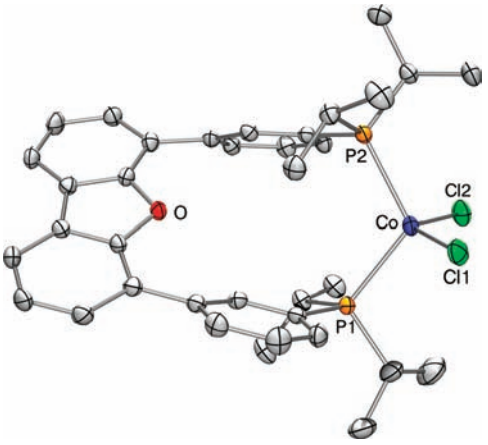

Figure 5. Solid-state structure of the [(^{iPr}DPDBFphos)$CoCl_2$] **2** at 50% probability level. Hydrogen atoms were omitted for clarity.

Theoretical Studies of (^{iPr}DPDBFphos)Ni^{I}Cl. DFT calculations were performed on the Ni(I) complex **4** using the BP86 and M06-L functionals. The optimized geometries compare favorably with the experimental structure (molecule *A*), whose coordinates were used as the initial geometry (Supporting Information, Table 3S). All calculated Ni−L bond distances are within 0.015 Å of their experimental values. The optimized bite angles were also remarkably close to the experimental value, differing at most by 2°.

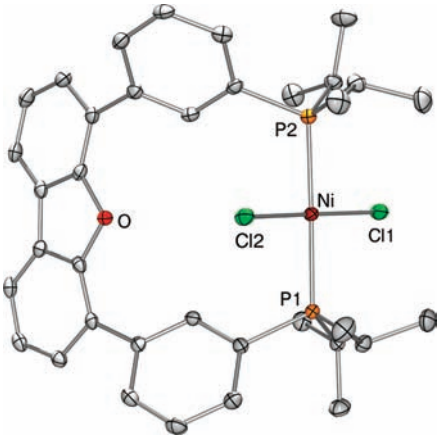

Figure 6. Solid-state structure of the [(^{iPr}DPDBFphos)$NiCl_2$] **3** at 50% probability level. Hydrogen atoms were omitted for clarity.

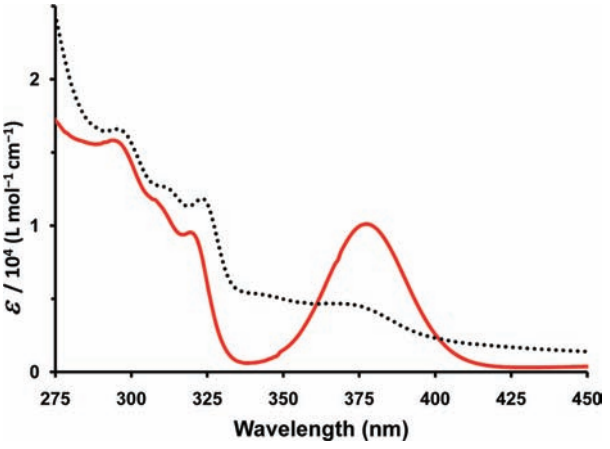

Figure 7. Electronic absorption spectra of the nickel compounds **3** (red solid line) and **4** (black dotted line) in THF at ambient temperature.

Scheme 2. Proposed Fluxional Processes in 3

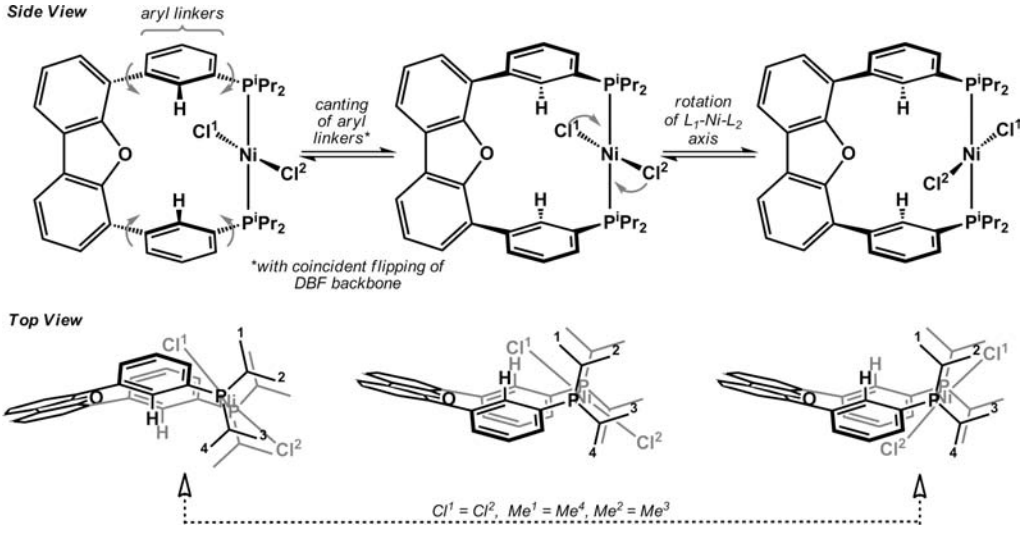

dx.doi.org/10.1021/ic200589e |*Inorg. Chem.* 2011, 50, 9290–9299

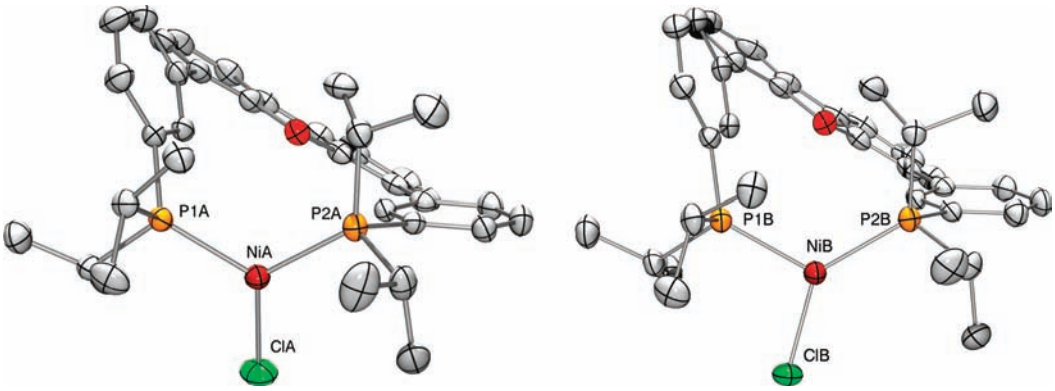

Figure 8. Solid-state structures of [(^{iPr}DPDBFphos)NiCl] **4** at 50% probability level. Both independent molecules in the unit cell are shown (*A*, left; *B*, right). Hydrogen atoms were omitted for clarity. Selected bond angles (deg): P1A−NiA−P2A 115.53(4), P1A−NiA−ClA 122.94(9), P2A−NiA−ClA 121.53(4), P1B−NiB−P2B 119.49(4), P1B−NiB−ClB 104.61(4), P2B−NiB−ClB 135.00(4).

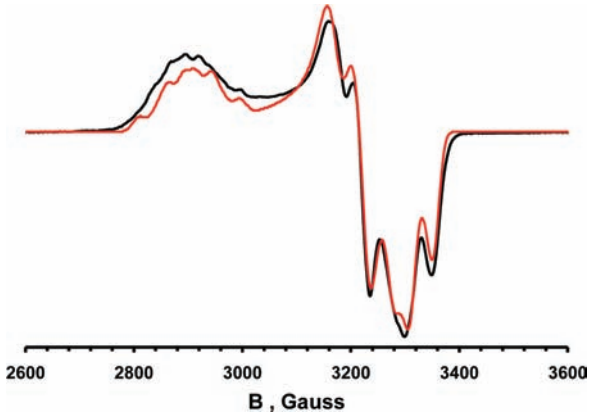

Figure 9. X-band EPR spectrum (dX''/dB) of Ni **4** in toluene glass shown in black (1 mM, 20.0 K, frequency = 9.65 GHz, modulation to 10.0 G, power = 0.02 mW). The spectrum was simulated (shown in red) by adopting the following values: g = (2.09, 2.14, 2.37); line widths, W = (12, 21, 13.5) G; A(two ^{31}P, I = 1/2) = (43, 40, 55) × 10^{-4} cm^{-1}; A(^{37}Cl/^{35}Cl, I = 3/2) = (12, 0.7, 35) × 10^{-4} cm^{-1}.

Figure 10 is the molecular-orbital (MO) diagram showing the splitting of the d-orbital manifold. Because the MO diagrams derived from the two functionals are very similar, only the results from the BP86 optimization are shown. For the following discussion, the molecular trigonal plane is defined as the *xy*-plane with the Ni−Cl vector along the *x*-axis. The d-orbital manifold comprises three energetically high-lying d-orbitals and two low-lying d-orbitals. The singly occupied MO (SOMO) is predominantly d_{xy} in composition and is σ-antibonding with respect to the phosphorus atoms and $\pi_{\|}$-antibonding with the chloride atom. This magnetic orbital description[55] is consistent with the EPR spectrum of **4**, which is characterized by a large hyperfine coupling constant to both phosphorus nuclei and a smaller interaction with the chloride nucleus. The next two MOs, which have d_{z^2} and d_{xz} parentage, are characterized by $\pi_{\perp}$-antibonding interactions with the chloride. Significantly lower in energy are the $d_{x^2-y^2}$ and d_{yz} orbitals. The former is slightly σ-antibonding with respect to chloride, and the latter is formally nonbonding. The calculated electronic structure is fully consistent with monovalent nickel. The lowest unoccupied MO (LUMO, not shown) is ligand-based and is characterized by delocalized

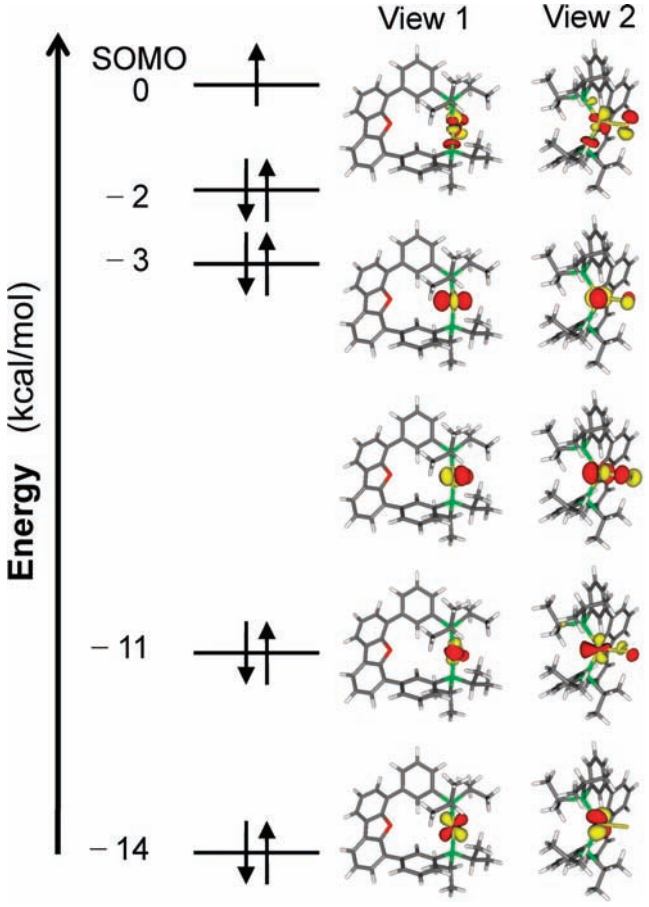

Figure 10. Qualitative MO diagram of the d-orbital manifold derived from a DFT-BP86 calculation of [(^{iPr}DPDBFphos)NiCl] **4**.

electron density throughout the π-system of the dibenzofuran backbone.

Reactivity Studies of (^{iPr}DPDBFphos)Ni^{I}Cl. Preliminary reactivity studies reveal that the Ni(I) complex **4** can cleave C−X bonds. Benzyl bromide and **4** react instantly at room temperature to yield bibenzyl (^{1}H NMR). The product mixture is characterized by a singularly broad signal in the ^{31}P NMR spectrum, which upon cooling to 0 °C resolves into three distinct peaks at 26.5,

dx.doi.org/10.1021/ic200589e |*Inorg. Chem.* 2011, 50, 9290–9299

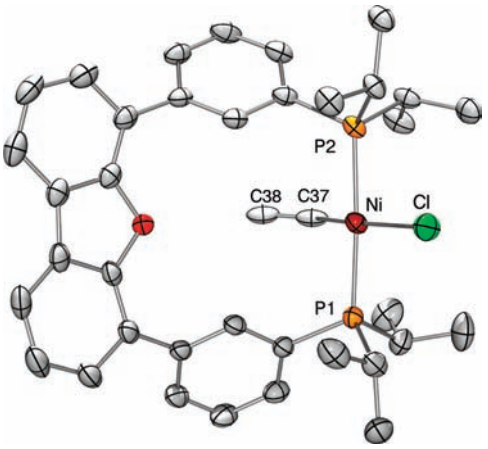

Figure 11. Solid-state structure of [(^{iPr}DPDBFphos)Ni(CH=CH_2)Cl] **6** at 50% probability level. Only one of the two independent molecules in the unit cell is shown. Hydrogen atoms were omitted for clarity. Selected bond lengths (Å) and angles (deg): Ni−P1 2.204(1), Ni−P2 2.210(1), Ni−Cl 2.241(1), Ni−C37 1.919(4), C37−C38 1.220(6), P1−Ni−P2 174.39(4), P1−Ni−Cl 93.35(4), P2−Ni−Cl 92.19(4), P1−Ni−C37 87.6(1), P2−Ni−C37 86.8(1), Ni−C37−C38 136.9(3).

29.0, and 31.2 ppm (Supporting Information, Figure 6S). The former corresponds to [*trans*-(^{iPr}DPDBFphos)$NiCl_2$] **3**. The latter two are assigned as the mixed halide [(^{iPr}DPDBFphos)NiClBr] and dibromide [(^{iPr}DPDBFphos)$NiBr_2$] compounds based on the following evidence. Metalation of (^{iPr}DPDBFphos) with $NiBr_2$ proceeds cleanly to [(^{iPr}DPDBFphos)$NiBr_2$] **5**. Complex **5** is characterized by a single peak at 31.2 ppm in the ^{31}P NMR spectrum at 0 °C, which matches well with that seen in the benzyl bromide reaction mixture. The third peak in the ^{31}P NMR spectrum at 29.0 ppm is presumably the mixed halide species [(^{iPr}DPDBFphos)NiClBr] because its chemical shift is exactly halfway between that of the nickel dichloride **3** and of the nickel dibromide **5** complexes.

Compound **4** reacts with excess vinyl chloride to cleanly produce [(^{iPr}DPDBFphos)$NiCl_2$] **3** and the vinyl complex, [(^{iPr}DPDBFphos)Ni(CH=CH_2)Cl] **6**, as identified by combustion analysis, ^{1}H NMR spectroscopy, and a single-crystal X-ray diffraction experiment (Figure 11, Table 1). The product ratio of **3**:**6** is 1:1 based on their relative integration in the ^{1}H NMR spectrum (Supporting Information, Figure 7S) and is consistent with the chemical equation,

$$2[(^{iPr}\text{DPDBFphos})Ni^{I}Cl] + CH_2{=}CHCl \rightarrow [(^{iPr}\text{DPDBFphos})Ni^{II}Cl_2] + [(^{iPr}\text{DPDBFphos})Ni^{II}(CH{=}CH_2)Cl]$$

Of interest, **4** also reacts with 1 equiv of vinyl bromide to generate a mixture that contains the Ni(II) dihalide complexes, **6**, and a new species that is assigned as the bromide analogue of **6** because of their similar spectroscopic data. Collectively, these results demonstrate that Ni(I) **4** cleaves vinyl−X bonds to ultimately produce stable Ni(II) products.

Two limiting mechanisms are proposed for the cleavage of vinyl halide: (1) a radical chain process is initiated by an inner-sphere electron transfer to form a Ni(II)-alkene adduct, Ni^{II}−(η^2-CH_2CHX)$^{\bullet-}$, which subsequently eliminates X$^\bullet$ and/or $CH_2CH^\bullet$, or (2) vinyl halide oxidatively adds to Ni(I) to produce a Ni(III) intermediate, $Ni^{III}X(CHCH_2)$, which then undergoes

Table 3. Kumada Cross-Coupling Reactions of Vinyl Chloride and PhMgBr[a]

entry	Ni source (5 mol %)	avg. yield (%)[b]	no. of runs
1	[(^{iPr}DPDBFphos)$Ni^{II}Cl_2$] **3**	66.4 ± 9.8	5
2	[(^{iPr}DPDBFphos)Ni^{I}Cl] **4**	85.9 ± 7.8	4
3	no nickel, no ligand	8.7 ± 7.7	4

[a] See Experimental Section for reaction conditions. [b] The yield of styrene is determined by GC-MS analysis.

comproportionation reactions with Ni(I). Though the assorted products in the reaction of **4** and vinyl bromide hint at radical processes, we cannot exclude the intermediacy of Ni(III) species.

Encouraged by the clean reactivity between **4** and vinyl chloride, we decided to investigate the catalytic potential of Ni(I) **4** in the original Kumada coupling reaction of vinyl chloride and phenyl Grignard reagent.[56] Using a loading of 5 mol % catalyst with excess vinyl chloride, both Ni(I) **4** and Ni(II) **3** generated styrene as the product in good yields (∼65 to 85%, Table 3, entries 1 and 2), with **4** slightly outperforming **3**. The control reaction (Table 3, entry 3) showed that no significant amount of styrene is formed under the same conditions in the absence of a catalyst.

Monovalent nickel species had long been proposed by Tsou and Kochi as intermediates in the nickel-catalyzed biaryl synthesis from aryl halides.[57] Indeed, mechanistic proposals for Ni-catalyzed cross-couplings commonly feature Ni(0), Ni(I), Ni(II), and Ni(III) species, which undergo one- and/or two-electron redox steps in the catalytic cycle.[25,58,59] Isolated monovalent nickel compounds have been found to be catalytically competent in various cross-coupling schemes.[30,31,60,61] In one case, the "nickel-(I)-terpyridine" catalyst was reformulated as a nickel(II) center bound to a reduced ligand radical based on EPR and DFT studies.[62] The other Ni(I) cross-coupling catalysts mostly have *N*-heterocyclic carbenes (NHCs) as ligands[30,31] and are considered to be bona fide Ni(I) species because metal-NHC complexes are not known to undergo ligand-based reductions (although NHCs can partake in π-backbonding).[63] To our knowledge, this report is the first comparative study between an isolated Ni(I)-phosphine complex and its Ni(II) analogue in a cross-coupling reaction.

III. CONCLUSIONS

The diphosphine ^{iPr}DPDBFphos was successfully used as a supporting ligand in tetrahedral Zn(II) and Co(II) complexes, as well as in square-planar Ni(II) and distorted trigonal planar Ni(I) compounds. The breadth of coordination geometries as exemplified by these complexes is enabled by the conformationally flexible backbone in ^{iPr}DPDBFphos. Compared to *cis*-chelating diphosphines, nonrigid *trans*-spanning diphosphines may be advantageous when a nonlabile ligand platform is required that must also accommodate different coordination geometries, such as during a catalytic cycle.

Given the limited evidence for Ni(I) in cross-coupling reactions, our results are intriguing in that a Ni(I) complex reacts constructively with vinyl−X bonds and is catalytically competent for the cross coupling of vinyl chloride and phenyl Grignard reagent. Definitive experimental proof for the direct involvement of monovalent nickel in cross-coupling catalysis is still lacking. The current results warrant further study of this Ni(I) system, especially to evaluate its scope in other cross-coupling schemes as

well as to scrutinize the role of Ni(I) through detailed mechanistic investigations.

IV. EXPERIMENTAL SECTION

Synthetic Considerations. Unless otherwise stated, all manipulations were performed under a dinitrogen atmosphere in a MBraun glovebox or using standard Schlenk techniques. Standard solvents were deoxygenated by sparging with dinitrogen and dried by passing through activated alumina columns of a SG Water solvent purification system. Deuterated solvents were purchased from Cambridge Isotope Laboratories, Inc., dried over CaH_2, distilled, and stored over activated 4 Å molecular sieves. Elemental analyses were performed by Atlantic Microlab. The synthesis of 4,6-bis(3-diisopropylphosphinophenyl)dibenzofuran, referred to as ^{iPr}DPDBFphos, was previously reported.[1] Other reagents were purchased commercially and used without further purification.

*Synthesis of [(^{iPr}DPDBFphos)ZnCl$_2$] (**1**).* A solution of zinc(II) chloride (0.026 g, 0.19 mmol) in 10 mL of THF was added dropwise to a solution of ^{iPr}DPDBFphos (0.102 g, 0.18 mmol) in 10 mL of THF. The reaction solution was stirred overnight. After 12 h, the solvent was removed under reduced pressure, and the resulting solids were washed with Et_2O and then extracted into THF. The THF solution was layered with hexane and stored at −35 °C overnight to give a white precipitate, which was collected and dried under reduced pressure (0.089 g, 70%). Single crystals suitable for X-ray diffraction analysis were grown from Et_2O. UV (THF) λ_{max}, nm (ε, L mol^{-1} cm^{-1}): 294 sh (13,000), 310 sh (6,400). ^{1}H NMR (500 MHz, $CDCl_3$): δ 8.33 (2H, br, CH), 8.03 (2H, d, J = 7.0 Hz, CH), 7.74 (2H, br. s, CH), 7.66 (2H, d, J = 6.5 Hz, CH), 7.62 (4H, m, J = 6.5 Hz, CH), 7.50 (2H, t, J = 7.5 Hz, CH), 2.59 (4H, m, PCH(CH$_3$)$_2$), 1.29 (12H, dd, J_{HH} = 8.0 Hz, J_{HP} = 15 Hz, PCH(CH_3)(C′H$_3$)), 1.19 (12H, dd, J_{HH} = 8.0 Hz, J_{HP} = 15 Hz, PCH(CH$_3$)(C′H_3)). ^{31}P NMR (121 MHz, $CDCl_3$): δ 2.7. ESI-MS-TOF m/z: [M − Cl]$^+$ calc. for $C_{36}H_{42}ClZnOP_2$, 651.1691; found, 651.3. Anal. Calcd. for $C_{36}H_{42}Cl_2OP_2Zn$: C, 62.76; H, 6.14; N, 0. Found: C, 60.82; H, 6.09; N, 0.0. Several different crystalline batches of **1** were tested, but no satisfactory analyses were obtained.

*Synthesis of [(^{iPr}DPDBFphos)CoCl$_2$] (**2**).* A suspension of cobalt(II) chloride (0.026 g, 0.20 mmol) in 20 mL of THF was added dropwise to a solution of ^{iPr}DPDBFphos (0.109 g, 0.20 mmol) in 20 mL of THF. The reaction solution was stirred overnight. After 12 h, the solvent was removed under reduced pressure, and the resulting solids were washed with Et_2O and then extracted into THF. The THF solution was filtered and then evaporated to dryness under reduced pressure to give a blue powder (0.133 g, 99%). Single crystals suitable for X-ray diffraction analysis were grown from Et_2O. UV−vis (THF) λ_{max}, nm (ε, L mol^{-1} cm^{-1}): 295 sh (16,000), 322 sh (7,600), 618 sh (500), 636 (530), 735 (320). ^{1}H NMR (300 MHz, C_6D_6): δ 21.36, 13.54, 7.95, 7.64, 6.79, 4.19, 1.83, −14.03. Evans' method ($CDCl_3$/$CHCl_3$, 300 MHz): μ_{eff} = 4.01 μ_B. Anal. Calcd. for $C_{36}H_{42}Cl_2OP_2Co$: C, 63.35; H, 6.20; N, 0. Found: C, 62.83; H, 6.05; N, 0.0.

*Synthesis of [(^{iPr}DPDBFphos)NiCl$_2$] (**3**).* A suspension of nickel(II) chloride (0.068 g, 0.52 mmol) in 20 mL of THF was added dropwise to a solution of ^{iPr}DPDBFphos (0.250 g, 0.45 mmol) in 20 mL. The reaction solution was heated at 70 °C with stirring. After 12 h, the solvent was removed under reduced pressure, and the resulting solids were washed with Et_2O and then extracted into THF. The THF solution was filtered and then stored at −35 °C overnight to give red crystals, which were collected and dried under reduced pressure (0.202 g, 65%). Single crystals suitable for X-ray diffraction analysis were grown from a CH_2Cl_2/Et_2O (1:3) solution. UV−vis (THF) λ_{max}, nm (ε, L mol^{-1} cm^{-1}): 295 sh (18,000), 322 sh (9,300), 377 (9,500), 487 (280). ^{1}H NMR (300 MHz, $CDCl_3$): δ 8.74 (2H, br, CH), 8.06 (2H, d, J = 7.5 Hz, CH), 7.57 (2H, d, J = 7.5 Hz, CH), 7.50 (6H, m, J = 7.5 Hz, CH), 7.13 (2H, br, CH), 2.75 (4H, br, PCH(CH$_3$)$_2$), 1.67 (12H, br, PCH(CH_3)(C′H$_3$)), 1.27 (12H, br, PCH(CH$_3$)(C′H_3)). ^{31}P NMR (121 MHz, $CDCl_3$): δ 26.5 (br). Anal. Calcd. for $C_{36}H_{42}Cl_2OP_2Ni$: C, 63.37; H, 6.20; N, 0. Found: C, 63.16; H, 6.20; N, 0.0.

*Synthesis of [(^{iPr}DPDBFphos)NiCl] (**4**).* A THF solution of **3** (0.095 g, 0.14 mmol) was added to KC_8 (0.020 g, 0.15 mmol) and stirred overnight. An immediate color change from red to yellow was observed. The reaction solution was filtered, and the filtrate was evaporated to dryness under reduced pressure. The resulting crude was dissolved in toluene, filtered, and then stored at −35 °C. The resulting yellow precipitate was collected and dried under reduced pressure (0.080 g, 90%). Single crystals suitable for X-ray diffraction analysis were obtained from a concentrated CD_3CN solution. UV (THF) λ_{max}, nm (ε, L mol^{-1} cm^{-1}): 263 (37,000), 298 (16,000), 314 sh (12,000), 324 (11,000), 346 sh (5,200), 375 (4,500). ^{1}H NMR (300 MHz, d$_8$-THF): δ 13.98, 9.03, 8.62, 7.97, 3.14. Anal. Calcd. for $C_{36}H_{42}ClOP_2Ni$: C, 66.85; H, 6.54; N, 0. Found: C, 67.00; H, 6.48; N, 0.0.

*Synthesis of [(^{iPr}DPDBFphos)NiBr$_2$] (**5**).* A suspension of nickel(II) bromide (0.134 g, 0.615 mmol) and ^{iPr}DPDBFphos (0.353 g, 0.638 mmol) in 20 mL of THF was heated to 70 °C with stirring for 9 h. Upon cooling to room temperature, the crude mixture was concentrated to 8 mL under reduced pressure, filtered through Celite, layered with 12 mL of pentane, and stored at −35 °C. Purple crystals formed overnight, and they were collected and dried under reduced pressure (0.297 g, 63%). ^{1}H NMR (400 MHz, CD_2Cl_2, −60 °C): δ 8.74 (2H, br, CH), 8.07 (2H, d, J = 7.5 Hz, CH), 7.62 (2H, d, J = 7.5 Hz, CH), 7.49 (6H, m, J = 7.5 Hz, CH), 7.29 (2H, br, CH), 2.81 (2H, br, PCH(CH$_3$)$_2$), 2.42 (2H, br, PC′H(CH$_3$)$_2$), 1.61 (12H, m, PCH(CH_3)$_2$), 1.19 (6H, m, PC′H(CH_3)(C′H$_3$)), 0.63 (6H, m, PC′H(CH$_3$)(C′H_3)). ^{31}P NMR (162 MHz, CD_2Cl_2, −60 °C): δ 30.3. ^{31}P NMR (162 MHz, d$_8$-THF, 0 °C): δ 31.2. Anal. Calcd. for $C_{36}H_{42}Br_2OP_2Ni$: C, 56.07; H, 5.49; N, 0. Found: C, 55.94; H, 5.59; N, 0.0.

*Synthesis of [(^{iPr}DPDBFphos)Ni(CHCH$_2$)Cl] (**6**).* A d$_8$-THF solution of **4** (0.017 g, 0.03 mmol) was added to a sealable NMR tube. The tube was frozen, evacuated, and refilled with excess vinyl chloride. An immediate color change was observed from yellow to orange red upon warming to room temperature. After 4 days at room temperature, the NMR spectra showed no starting material and two different products; complexes **3** and **6**, present in a 1:1 ratio. Complex **6** was synthesized independently through the reaction of vinyl chloride and a nickel(0) complex. Single crystals suitable for X-ray diffraction analysis were grown from a THF/Pentane (1:2) solution. UV−vis (THF) λ_{max}, nm (ε, L mol^{-1} cm^{-1}): 285 (32,000), 308 sh (19,000), 318 sh (15,000), 430 (700). ^{1}H NMR (500 MHz, d$_8$-THF): δ 8.50 (2H, m, CH), 8.12 (2H, dd, J = 1.5 and 8.0 Hz, CH), 7.62 (2H, d, J = 8.0 Hz, CH), 7.58 (2H, dd, J = 1.5 and 8.0 Hz, CH), 7.50 (2H, t, J = 8.0 Hz, CH), 7.49 (2H, t, J = 8.0 Hz, CH), 7.36 (2H, m, CH), 5.91 (1H, ddt, J_{HH} = 10.2 and 17.5 Hz, J_{HP} = 5.5 Hz, NiCH = CHH′), 4.42 (1H, dt, J_{HH} = 17.5 Hz, J_{HP} = 3.0 Hz, *cis*-NiCH=CHH′), 4.14 (1H, dt, J_{HH} = 10.2 Hz, J_{HP} = 4.5 Hz, *trans*-NiCH=CHH′), 2.96 (2H, m, PCH(CH$_3$)$_2$), 2.73 (2H, m, PC′H(CH$_3$)$_2$), 1.64 (6H, dd, J_{HH} = 7.0 Hz, J_{HP} = 14.0 Hz, PC′H(CH_3)(C′H$_3$)), 1.62 (6H, dd, J_{HH} = 7.5 Hz, J_{HP} = 15.0 Hz, PC′H(CH$_3$)(C′H_3)), 1.36 (6H, dd, J_{HH} = 7.5 Hz, J_{HP} = 15.5 Hz, PCH(CH_3)(C′H$_3$)), 0.71 (6H, dd, J_{HH} = 6.0 Hz, J_{HP} = 12.0 Hz, PCH(CH$_3$)(C′H_3)). ^{31}P NMR (121 MHz, d$_8$-THF): δ 29.1. Anal. Calcd. for $C_{38}H_{45}ClOP_2Ni$: C, 67.73; H, 6.73; N, 0. Found: C, 67.97; H, 6.89; N, 0.0.

General Procedure for Kumada Coupling Reactions. A THF solution of the Ni catalyst (0.003 mmol, 2.14 mL) was added to a sealable reaction flask equipped with a magnetic stir bar, and the solution was frozen with a glovebox LN_2 coldwell bath. Once frozen, a solution of phenylmagnesium bromide (0.06 mmol, 0.02 mL, 3.0 M in Et_2O) diluted with Et_2O (0.84 mL) was added on top and frozen as a separate layer. The reaction flask was then evacuated and charged with excess vinyl chloride. Reactions were allowed to thaw and stir for 22 h at room temperature. The reaction was quenched by adding 2 mL of Et_2O

dx.doi.org/10.1021/ic200589e |*Inorg. Chem.* 2011, 50, 9290–9299

and 4 mL of 1.0 M HCl to the solution. The organic layer was extracted, dried over $MgSO_4$ and filtered. The filtrate was analyzed on the GC-MS. Yields were calculated using GC-MS peak integrations and a styrene-standard calibration curve.

X-ray Crystallographic Data Collection and Refinement of the Structures. A colorless plate of **1**, a blue block of **2**, a red plate of **3**, a yellow plate of **4**, and a yellow block of **6** were placed onto the tip of a 0.1 mm diameter glass capillary and mounted on a Bruker or a Siemens SMART Platform CCD diffractometer for data collection at 173(2) K for complexes **1**, **2**, and **4**, or 123(2) K for complexes **3** and **6**. The data collection was carried out using Mo Kα radiation (graphite monochromator). The data intensity was corrected for absorption and decay (SADABS). Final cell constants were obtained from least-squares fits of all measured reflections. The structure was solved using SHELXS-97 and refined using SHELXL-97. A direct-methods solution was calculated which provided most non-hydrogen atoms from the E-map. Full-matrix least-squares/difference Fourier cycles were performed to locate the remaining non-hydrogen atoms. All non-hydrogen atoms were refined with anisotropic displacement parameters. Hydrogen atoms were placed in ideal positions and refined as riding atoms with relative isotropic displacement parameters. For **6**, a highly disordered THF molecule could not be modeled appropriately and was removed using the PLATON program, SQUEEZE function.[64] A total of 46 electrons in a volume of 353 Å^3 located at (0.5, 1, 0) in the unit cell were determined. Crystallographic data for **1**−**4** and **6** are summarized in Table 1.

Physical Measurements. ^{1}H and ^{31}P NMR spectra were acquired on Varian Inova 300 and 500 MHz spectrometers at ambient temperature unless otherwise stated. Chemical shifts were referenced to residual solvent in ^{1}H NMR spectra, while ^{31}P NMR spectra were referenced to an external reference of 85% H_3PO_4 set to 0 ppm. For **6**, proton assignments were based on a COSY NMR experiment. Solution magnetic susceptibilities were determined by the Evans method[65,66] and were corrected for underlying diamagnetism using tabulated Pascal's constants.[67] Electronic spectra of complexes were recorded on a Cary 300 Bio UV−visible spectrophotometer. Perpendicular-mode X-band EPR spectra were recorded on a Bruker EPP 300 spectrometer equipped with an Oxford ESR 910 liquid helium cryostat and an Oxford temperature controller. X-band EPR spectra were simulated using EPR program (version W95) written by Professor Frank Neese (University of Bonn, Germany). Cyclic voltammetry experiments were performed inside a glovebox with a CHInstruments Model 600D potentiostat/galvanostat. A single-chamber cell was set up with a glassy carbon working electrode (3 mm diameter), a Pt wire as the auxiliary electrode, and a reference electrode consisting of a silver wire in 10 mM $AgNO_3$ solution (0.1 M $[^nBu_4N]PF_6$ in CH_3CN). All measurements were calibrated to an internal ferrocene standard. Mass spectrometry (MS) data were acquired on a Bruker BioTOF ESI-MS under positive mode.

Theoretical Calculations. DFT calculations (BP86,[68,69] M-06 L[70,71]) were performed with the Gaussian09 program.[72] The all-electron Gaussian basis sets used were those reported by the Ahlrichs group.[73] For nickel, chloride, and phosphorus atoms, the triple-ζ-quality basis sets with one set of polarization functions was used (def2-TZVP). The carbon, oxygen, and hydrogen atoms were described by smaller polarized split-valence def2-SV(P) basis sets.

■ ASSOCIATED CONTENT

Ⓢ Supporting Information. Additional spectroscopic and theoretical data, including Beer's Law plots for **1**−**3**, the ^{1}H NMR spectrum of $[(^{iPr}$DPDBFphos$)ZnCl_2]$ **1**, cyclic voltammograms of **1**− **4**, the *xyz* file for the geometry optimized structure of **4**, the ^{1}H NMR and UV−vis spectra of **6**. This material is available free of charge via the Internet at http://pubs.acs.org.

■ AUTHOR INFORMATION

Corresponding Author
*E-mail: clu@umn.edu.

■ ACKNOWLEDGMENT

E.E.M. thanks Professor Kris McNeill (ETH Zürich) and the NSF (CHE-0809575 and 0952054) for support. S.J.T. thanks 3M for a graduate fellowship. The Lando-NSF Summer Research Program is gratefully acknowledged for giving J.E.M. financial support. Dr. Victor Young, Jr. (X-ray Crystallographic Laboratory) and Dr. Yuming Zhou provided assistance with X-ray crystallography and acquiring EPR spectra, respectively. We thank Professors William Tolman and John Lipscomb for the generous use of their GC/MS and EPR instruments, respectively. Computing support and resources were provided by the Minnesota Supercomputing Institute, and partial funding for this work was given by the Initiative for Renewable Energy and the Environment (U of M).

■ REFERENCES

(1) Ding, K.; Miller, D. L.; Young, V. G., Jr.; Lu, C. C. *Inorg. Chem.* **2011**, *50*, 2545–2552.
(2) Haenel, M. W.; Jakubik, D.; Rothenberger, E.; Schroth, G. *Chem. Ber.* **1991**, *124*, 1705–1710.
(3) Kranenburg, M.; van der Burgt, Y. E. M.; Kamer, P. C. J.; van Leeuwen, P. W. N. M.; Goubitz, K.; Fraanje, J. *Organometallics* **1995**, *14*, 3081–3089.
(4) Jiménez-Rodríguez, C.; Roca, F. X.; Bo, C.; Benet-Buchholz, J.; Escudero-Adán, E. C.; Freixa, Z.; van Leeuwen, P. W. N. M. *Dalton Trans.* **2006**, 268–278.
(5) Fairlamb, I. J. S.; Tommasi, S.; Moulton, B. E.; Zheng, W.; Lin, Z.; Whitwood, A. C. *Eur. J. Inorg. Chem.* **2007**, *2007*, 3173–3178.
(6) Allen, F. *Acta Crystallogr., Sect. B* **2002**, *58*, 380–388.
(7) Orpen, A. G. *Acta Crystallogr., Sect. B* **2002**, *58*, 398–406.
(8) Kulkarni, A. A.; Daugulis, O. *Synthesis* **2009**, *2009*, 4087–4109.
(9) Bullock, R. M., Ed.; *Catalysis Without Precious Metals*; Wiley-VCH: Weinheim, Germany, 2010.
(10) Fürstner, A.; Leitner, A.; Méndez, M.; Krause, H. *J. Am. Chem. Soc.* **2002**, *124*, 13856–13863.
(11) Traylor, T. G.; Hill, K. W.; Fann, W.-P.; Tsuchiya, S.; Dunlap, B. E. *J. Am. Chem. Soc.* **1992**, *114*, 1308–1312.
(12) Costas, M.; Que, L., Jr. *Angew. Chem., Int. Ed.* **2002**, *41*, 2179–2181.
(13) Britovsek, G. J. P.; England, J.; White, A. J. P. *Dalton Trans.* **2006**, 1399–1408.
(14) Chen, M. S.; White, M. C. *Science* **2007**, *318*, 783–787.
(15) Bianchini, C.; Meli, A.; Peruzzini, M.; Frediani, P.; Bohanna, C.; Esteruelas, M. A.; Oro, L. A. *Organometallics* **1992**, *11*, 138–145.
(16) Bart, S. C.; Lobkovsky, E.; Chirik, P. J. *J. Am. Chem. Soc.* **2004**, *126*, 13794–13807.
(17) Daida, E. J.; Peters, J. C. *Inorg. Chem.* **2004**, *43*, 7474–7485.
(18) Morris, R. H. *Chem. Soc. Rev.* **2009**, *38*, 2282–2291.
(19) Bullock, R. M. *Angew. Chem., Int. Ed.* **2007**, *46*, 7360–7363.
(20) Hebrard, F.; Kalck, P. *Chem. Rev.* **2009**, *109*, 4272–4282.
(21) Gosmini, C.; Moncomble, A. *Isr. J. Chem.* **2010**, *50*, 568–576.
(22) Keim, W. *Angew. Chem., Int. Ed. Engl.* **1990**, *29*, 235–244.
(23) Younkin, T. R.; Connor, E. F.; Henderson, J. I.; Friedrich, S. K.; Grubbs, R. H.; Bansleben, D. A. *Science* **2000**, *287*, 460–462.
(24) Ittel, S. D.; Johnson, L. K.; Brookhart, M. *Chem. Rev.* **2000**, *100*, 1169–1204.
(25) Rosen, B. M.; Quasdorf, K. W.; Wilson, D. A.; Zhang, N.; Resmerita, A.-M.; Garg, N. K.; Percec, V. *Chem. Rev.* **2010**, *111*, 1346–1416.
(26) Negishi, E. *Bull. Chem. Soc. Jpn.* **2007**, *80*, 233–257.
(27) Montgomery, J. *Angew. Chem., Int. Ed.* **2004**, *43*, 3890–3908.
(28) Castro, P. M.; Lankinen, M. P.; Leskelä, M.; Repo, T. *Macromol. Chem. Phys.* **2005**, *206*, 1090–1097.

(29) Kim, H. S.; Bae, J. Y.; Lee, J. S.; Kwon, O.-S.; Jelliarko, P.; Lee, S. D.; Lee, S.-H. *J. Catal.* **2005**, *232*, 80–84.
(30) Miyazaki, S.; Koga, Y.; Matsumoto, T.; Matsubara, K. *Chem. Commun.* **2010**, *46*, 1932–1934.
(31) Zhang, K.; Conda-Sheridan, M.; Cooke, S. R.; Louie, J. *Organometallics* **2011**, *30*, 2546–2552.
(32) Chadwell, S. J.; Coles, S. J.; Edwards, P. G.; Hursthouse, M. B.; Imran, A. *Polyhedron* **1995**, *14*, 1057–1065.
(33) The methyl group protons appear as three multiplets with relative integrations of 2:1:1. Upon close inspection, the splitting pattern of the two smaller signals are pseudo quartets (1:2:2:1), while for the larger signal, a pseudo quintet is seen. The pseudo quintet is rationalized as a coincident overlap of two pseudo quartets, which could potentially give rise to a more complicated 1:4:6:4:1 splitting pattern (see Figure 3, inset).
(34) Jolly, P. W.; Jonas, K.; Krüger, C.; Tsay, Y.-H. *J. Organomet. Chem.* **1971**, *33*, 109–122.
(35) Aresta, M.; Nobile, C. F.; Albano, V. G.; Forni, E.; Manassero, M. *J. Chem. Soc., Chem. Commun.* **1975**, 636–637.
(36) Mindiola, D. J.; Hillhouse, G. L. *J. Am. Chem. Soc.* **2002**, *124*, 9976–9977.
(37) Mindiola, D. J.; Hillhouse, G. L. *J. Am. Chem. Soc.* **2001**, *123*, 4623–4624.
(38) Melenkivitz, R.; Mindiola, D. J.; Hillhouse, G. L. *J. Am. Chem. Soc.* **2002**, *124*, 3846–3847.
(39) Ingleson, M. J.; Fullmer, B. C.; Buschhorn, D. T.; Fan, H.; Pink, M.; Huffman, J. C.; Caulton, K. G. *Inorg. Chem.* **2007**, *47*, 407–409.
(40) Bai, G.; Wei, P.; Stephan, D. W. *Organometallics* **2005**, *24*, 5901–5908.
(41) Holland, P. L.; Cundari, T. R.; Perez, L. L.; Eckert, N. A.; Lachicotte, R. J. *J. Am. Chem. Soc.* **2002**, *124*, 14416–14424.
(42) Puiu, S. C.; Warren, T. H. *Organometallics* **2003**, *22*, 3974–3976.
(43) Hu, X.; Castro-Rodriguez, I.; Meyer, K. *Chem. Commun.* **2004**, 2164–2165.
(44) Schaub, T.; Backes, M.; Radius, U. *Organometallics* **2006**, *25*, 4196–4206.
(45) Schmedake, T. A.; Haaf, M.; Paradise, B. J.; Powell, D.; West, R. *Organometallics* **2000**, *19*, 3263–3265.
(46) Kogut, E.; Wiencko, H. L.; Zhang, L.; Cordeau, D. E.; Warren, T. H. *J. Am. Chem. Soc.* **2005**, *127*, 11248–11249.
(47) (a) Bai, G.; Stephan, D. W. *Angew. Chem., Int. Ed.* **2007**, *46*, 1856–1859. (b) Iluc, V. M.; Miller, A. J. M.; Anderson, J. S.; Monreal, M. J.; Mehn, M. P.; Hillhouse, G. L. *J. Am. Chem. Soc.* **2011**, *133*, 13055–13063.
(48) Rowland, R. S.; Taylor, R. *J. Phys. Chem.* **1996**, *100*, 7384–7391.
(49) To find short non-bonded contacts, the C-H bonds in both independent molecules were first normalized to 1.083 Å. For the distorted molecule *B*, no short bond contact near the Cl atom was found below the 2.88 Å benchmark. Unexpectedly, the Cl atom in the undistorted molecule *A* had three contacts within 2.88 Å (Supporting Information, Table 2S). We draw the conclusion that short-bonded contacts near the chloride atom are not responsible for its asymmetric position between the two P atoms.
(50) Norman, N. C.; Orpen, A. G.; Quayle, M. J.; Whittell, G. R. *Acta Crystallogr., Sect. C* **2002**, *58*, m160–m161.
(51) Langer, J.; Fischer, R.; Görls, H.; Theyssen, N.; Walther, D. *Z. Anorg. Allg. Chem.* **2007**, *633*, 557–562.
(52) Eckert, N. A.; Dinescu, A.; Cundari, T. R.; Holland, P. L. *Inorg. Chem.* **2005**, *44*, 7702–7704.
(53) (a) Bai, G.; Wei, P.; Stephan, D. W. *Organometallics* **2005**, *24*, 5901–5908. (b) Saraev, V. V.; Kraikivskii, P. B.; Svoboda, I.; Kuzakov, A. S.; Jordan, R. F. *J. Phys. Chem. A* **2008**, *112*, 12449–12455.
(54) Nilges, M. J.; Barefield, E. K.; Belford, R. L.; Davis, P. H. *J. Am. Chem. Soc.* **1977**, *99*, 755–760.
(55) Kahn, O.; Prins, R.; Reedijk, J.; Thompson, J. S. *Inorg. Chem.* **1987**, *26*, 3557–3561.
(56) Tamao, K.; Sumitani, K.; Kumada, M. *J. Am. Chem. Soc.* **1972**, *94*, 4374–4376.
(57) Tsou, T. T.; Kochi, J. K. *J. Am. Chem. Soc.* **1979**, *101*, 7547–7560.
(58) Gómez-Benítez, V.; Baldovino-Pantaleón, O.; Herrera-Álvarez, C.; Toscano, R. A.; Morales-Morales, D. *Tetrahedron Lett.* **2006**, *47*, 5059–5062.
(59) Amatore, C.; Jutand, A. *Organometallics* **1988**, *7*, 2203–2214.
(60) Jones, G. D.; McFarland, C.; Anderson, T. J.; Vicic, D. A. *Chem. Commun.* **2005**, 4211–4213.
(61) Phapale, V. B.; Buñuel, E.; García-Iglesias, M.; Cárdenas, D. J. *Angew. Chem., Int. Ed.* **2007**, *46*, 8790–8795.
(62) Jones, G. D.; Martin, J. L.; McFarland, C.; Allen, O. R.; Hall, R. E.; Haley, A. D.; Brandon, R. J.; Konovalova, T.; Desrochers, P. J.; Pulay, P.; Vicic, D. A. *J. Am. Chem. Soc.* **2006**, *128*, 13175–13183.
(63) Hu, X.; Castro-Rodriguez, I.; Olsen, K.; Meyer, K. *Organometallics* **2004**, *23*, 755–764.
(64) Spek, A. L. *Acta Crystallogr.* **1990**, *A46*, C34.
(65) Schubert, E. M. *J. Chem. Educ.* **1992**, *69*, 62.
(66) Evans, D. F.; Fazakerley, G. V.; Phillips, R. F. *J. Chem. Soc. A* **1971**, 1931–1934.
(67) Bain, G. A.; Berry, J. F. *J. Chem. Educ.* **2008**, *85*, 532–536.
(68) Becke, A. D. *Phys. Rev. A* **1988**, *38*, 3098–3100.
(69) Perdew, J. P. *Phys. Rev. B* **1986**, *33*, 8822–8824.
(70) Zhao, Y.; Truhlar, D. G. *Acc. Chem. Res.* **2008**, *41*, 157–167.
(71) Zhao, Y.; Truhlar, D. G. *J. Chem. Phys.* **2006**, *125*, 194101–194118.
(72) Frisch, M. J.; Trucks, G. W.; Schlegel, H. B.; Scuseria, G. E.; Robb, M. A.; Cheeseman, J. R.; Scalmani, G.; Barone, V.; Mennucci, B.; Petersson, G. A.; Nakatsuji, H.; Caricato, M.; Li, X.; Hratchian, H. P.; Izmaylov, A. F.; Bloino, J.; Zheng, G.; Sonnenberg, J. L.; Hada, M.; Ehara, M.; Toyota, K.; Fukuda, R.; Hasegawa, J.; Ishida, M.; Nakajima, T.; Honda, Y.; Kitao, O.; Nakai, H.; Vreven, T.; J. A. Montgomery, J.; Peralta, J. E.; Ogliaro, F.; Bearpark, M.; Heyd, J. J.; Brothers, E.; Kudin, K. N.; N.Staroverov, V.; Kobayashi, R.; Normand, J.; Raghavachari, K.; Rendell, A.; Burant, J. C.; Iyengar, S. S.; Tomasi, J.; Cossi, M.; Rega, N.; Millam, J. M.; Klene, M.; Knox, J. E.; Cross, J. B.; Bakken, V.; Adamo, C.; Jaramillo, J.; Gomperts, R.; Stratmann, R. E.; Yazyev, O.; Austin, A. J.; Cammi, R.; Pomelli, C.; Ochterski, J. W.; Martin, R. L.; Morokuma, K.; Zakrzewski, V. G.; Voth, G. A.; Salvador, P.; Dannenberg, J. J.; Dapprich, S.; Daniels, A. D.; Farkas, O.; Foresman, J. B.; Ortiz, J. V.; Cioslowski, J.; Fox, D. J. *Gaussian 09*, Revision A.02; Gaussian, Inc.: Wallingford, CT, 2009.
(73) Weigend, F.; Ahlrichs, R. *Phys. Chem. Chem. Phys.* **2005**, *7*, 3297–3305.